DOI: 10.4408/IJEGE.2021-01.S-05

BIVARIATE LANDSLIDE SUSCEPTIBILITY ANALYSIS IN THE LORESTAN ARC (ZAGROS MOUNTAINS, IRAN)

Michele DELCHIARO(*), Javad ROUHI(*), Mario VALIANTE(**), Marta DELLA SETA(*), Carlo ESPOSITO(*) & Salvatore MARTINO(*)

(*)Sapienza University of Rome - Earth Sciences Department - Rome, Italy
(**)University of Salerno - Department of Civil Engineering - Fisciano, Italy
Corresponding author: michele.delchiaro@uniroma1.it

EXTENDED ABSTRACT

Nelle regioni tettonicamente attive, le frane sono uno dei più importanti processi di modellazione del paesaggio. A seconda della tipologia e della cinematica di frana, questi processi possono evolvere con velocità variabili, interessare materiali diversi e mobilitare volumi differenti. In generale, la topografia (pendenza, esposizione, energia di rilievo, curvatura, ecc.) e la litologia sono considerati fattori condizionanti (preparatori e predisponenti), mentre le precipitazioni, gli eventi sismici ed il contributo antropico sono noti come fattori scatenanti.

In questo senso, le frane costituiscono gravi rischi ambientali con impatti sociali, economici e naturali su larga scala e le mappe di suscettibilità sono strumenti chiave per la pianificazione, la gestione e la mitigazione del rischio. La suscettibilità da frana è definita come la probabilità spaziale del verificarsi di una frana, basata sulle condizioni locali del terreno. Essa valuta la relazione quantitativa tra più fattori di controllo e il verificarsi del fenomeno. La previsione spaziale delle frane sotto forma di studi di valutazione della suscettibilità è stata applicata negli ultimi 30 anni e nuove tecniche vengono continuamente sviluppate e aggiornate.

L'approccio statistico Bayesiano nello studio di suscettibilità da frana, come il Frequency Ratio (FR) oggetto del presente lavoro, è riconosciuto come metodo consono alla zonazione regionale, fornendo in prima istanza il contributo di ciascun fattore di condizionamento.

I monti Zagros (Iran) sono rinomati tra gli esempi più spettacolari di evoluzione del paesaggio adattata all'erodibilità dei litotipi affioranti in risposta alla crescita delle strutture a pieghe come fattori predisponenti per i movimenti gravitativi. In questo contesto geomorfologico, anche l'intensa sismicità associata all'attività delle principali faglie regionali (per esempio Main Zagros Reverse Fault, High Zagros Fault, Balarud Fault e Mountain Front Fault) costituisce un possibile innesco di movimenti gravitativi. Ciononostante, non è presente un inventario di frane per la catena degli Zagros, tanto meno per la regione del Lorestan, dove la frana più grande sulla terra emersa (44 km^3), è avvenuta circa 10.000 anni fa.

A questo proposito, l'obiettivo del presente lavoro è stato uno studio conoscitivo preliminare della suscettibilità bivariata da frana calcolata alla scala del pixel del digital elevation model (DEM) utilizzato nelle analisi (SRTM a 30 m). Nello specifico, l'analisi è stata realizzata basandosi su un inventario inedito delle frane nella regione del Lorestan. L'analisi di suscettibilità è stata eseguita solo sulle categorie a) "Crolli" (323) e b) "Scorrimenti" (297) il cui numero è stato ritenuto consistente, a differenza delle altre categorie. È stata quindi quantificata la sensibilità delle tipologie di frane a un insieme di parametri predisponenti riconducibili a 2 macrocategorie: a) fattori statici, di natura morfologica, idraulica e geologica e b) fattori pseudo-dinamici o potenzialmente innescanti in termini medi sul lungo periodo che cumula, dunque, gli effetti delle forze tettoniche transienti dei singoli eventi sismici in riferimento agli effetti morfotettonici sul sistema versante-fondovalle.

La significatività statistica dei fattori pseudo-dinamici è stata dimostrata dapprima tramite la regressione logistica univariata ad un insieme di punti "stabili" e "instabili" generato casualmente. Quindi sono stati costruiti i modelli di suscettibilità ed è stata determinata l'importanza di ogni fattore di condizionamento calcolando il contributo dei fattori nel determinare il valore medio dell'indice di suscettibilità frana nelle frane reali, e la percentuale di casi di frana in cui il rapporto di frequenza relativo a ciascuna variabile è maggiore di 1.

Per quanto riguarda la categoria "Crolli", il modello evidenzia molto bene come suscettibili le zone con angolo di inclinazione maggiore di 38°, associate ad un'energia di rilievo (calcolata per un raggio di 5000 m) di 1100-1550 m una distanza di faglia mediana di circa 10 km. Il modello di suscettibilità ottenuto per la categoria "Scorrimenti" mostra invece una forte propensione al dissesto con valori di angolo di pendenza compresi tra 18°-35°, con l'affioramento dei litotipi più resistenti come il calcare e il calcare marnoso, in particolare in corrispondenza di morfologie come i "flat irons". L'accuratezza del modello risultante, convalidata con la curva del tasso di predizione su un set di dati campione non utilizzato nell'analisi di suscettibilità, è 0,94 per i "Crolli" e 0,77 per gli "Scorrimenti", indicando una buona accuratezza della previsione.

ABSTRACT

Landslide susceptibility analysis based on the assessment of a quantitative relationship between multiple controlling factors and landslide occurrence is a consolidated approach for land-use planning in risk mitigation. The Zagros Mountain range (Iran) is one of the most spectacular examples of a landscape whose evolution has been controlled by the erosion of rock outcrops and the growth of thrust-fold structures (predisposing factors for gravity-driven deformations).

This paper covers a preliminary study on the landslide susceptibility of the Lorestan region of the Zagros Mountains. Use was made of a bivariate Frequency Ratio, computed on a 30 m pixel size Shuttle Radar Topography Mission Digital Elevation Model. In particular, reliance was made on an unpublished inventory of landslides in the Lorestan Arc. Landslide susceptibility was assessed in the "Falls" (323) and "Slides" (297) categories, the numbers of which (unlike those of other categories) were regarded as suitable for robust modelling. A multi-parametric analysis was carried out to determine the susceptibility of each type of landslide to a set of contributing factors. These factors, most of which are commonly used in the literature, can be grouped in two main categories: a) static, including morphological, hydraulic, and geological factors, and b) pseudo-dynamic, including distance from active faults and steepness index (ksn), a morphometric tectonic uplift proxy computed along stream networks. The latter were considered as potentially landslide-triggering factors in the medium-long term, combining both the effects of transient tectonic forces of individual seismic events and morphotectonic effects on the slope-valley system. The statistical significance of these pseudo-dynamic factors was initially demonstrated via a univariate logistic regression with a randomly generated set of "stable" and "unstable" points. Then, models were built, and the importance of each conditioning factor was assessed by calculating the contribution of the factors in determining the mean landslide susceptibility index value in actual landslides, and the percentage of landslide cases in which the frequency ratio relative to each variable was above 1.

With regard to the "Falls" category, the model showed (with a high reliability) that susceptible areas were those with a slope angle greater than 38°, associated with a 5000 m radius relief energy of about 1100-1550 m and a median fault distance of about 10 km. Conversely, the susceptibility model obtained for the "Slides" category showed that highly susceptible areas were those with slope angle values of 18°-35° and featuring outcrops of the most resistant lithotypes, such as limestone and marly limestone, especially close to flatiron landforms. The resulting model accuracy (validated with the prediction rate curve method on a sample dataset not used in the susceptibility analysis), was equal to 0.94 for "Falls" and 0.77 for "Slides", indicating a good prediction accuracy.

***Keywords**: Frequency Ratio, landslide susceptibility, bivariate analysis, steepness index, Zagros Mountains*

INTRODUCTION

Landslides are one of the most important land-shaping processes that affect tectonically active regions in response to gravitational instabilities of hillslopes (Montgomery & Brandon, 2002; Agliardi *et alii*, 2009; Korup *et alii*, 2010; Larsen & Montgomery, 2012). Depending on the type of landslide and the slope failure kinematics, these processes can evolve with different velocities, affect different materials, and mobilise variable volumes (e.g., Hungr *et alii*, 2014). In general, topography (slope, aspect, relief, curvature, etc.) and lithology are considered as conditioning (preparatory and predisposing) factors, while rainfall, earthquakes, and anthropogenic elements are known as triggering factors (e.g. Pourghasemi *et alii*, 2018).

However, landslides constitute severe environmental hazards with large-scale social, economic, and natural impacts (Guzzetti *et alii*, 1999; Parise & Jibson, 2000; Pourghasemi *et alii*, 2018), and susceptibility maps are key tools for land-use planning, management, and risk mitigation (e.g. Trigila, 2013).

Landslide susceptibility is defined as the spatial probability of landslide occurrence, based on local terrain conditions (e.g. Guzzetti *et alii*, 1999; Mergili *et alii*, 2014). Spatial prediction of landslides in the form of susceptibility assessment studies has been applied for the past 30 years, and new techniques are continuously being developed and updated (Hussin *et alii*, 2016; Reichenbach *et alii*, 2018). Landslide susceptibility can be determined by using statistical and physically based models (Guzzetti *et alii*, 1999; Van Westen, 2000; Guzzetti, 2006, Van Westen *et alii*, 2006).

Among data-driven methods, statistically based techniques for landslide susceptibility evaluation have been preferred so far (Reichenbach *et alii*, 2018; Samia *et alii*, 2020). Among the wide array of available statistical methods, ranging from simple bivariate to sophisticated multivariate and machine learning approaches, the choice should be based on the scale of the study, the input data accuracy and, above all, the final aim of the analysis. With regard to analyses concerning large areas and involving zoning at the regional scale, basic zoning methods and preliminary zoning levels are recommended (Cascini, 2008). In recent years, many landslide susceptibility maps have been produced by using GIS-based statistical approaches, e.g. Frequency Ratio (FR) and Weights of Evidence (WoE) models (e.g. Mersha & Meten, 2020). The results from these models show good performance with high accuracy; these models, which are easy to use, can also provide the contribution of each conditioning factor to landslide occurrence (e.g. Lee & Pradhan, 2007; Vakhshoori & Zare, 2016).

The Zagros Mountain range (Iran) is one of the most

spectacular examples of a landscape whose evolution has been determined by the erosion of rock outcrops and the growth of thrust-fold structures (Ramsey *et alii*, 2008), representing predisposing factors for gravity-driven deformations (Rouhi *et alii*, 2019; Delchiaro *et alii* 2019 a, b, 2020 a, b). However, no landslide inventory is available for this mountain range, which includes the Lorestan region, in which the giant Seymareh landslide - the largest landslide (44 km^3) on the Earth's surface - occurred about 10,000 years ago (Roberts & Evans, 2013; Rouhi *et alii*, 2019; Delchiaro *et alii*, 2019 a, b, 2020a). In this geomorphological setting, intense seismicity associated with the activity of the main regional faults (i.e. Main Zagros Reverse Fault, High Zagros Fault, Balarud Fault, and Mountain Front Fault) can also trigger slope instabilities.

The study reported in this paper relied on an unpublished inventory of landslides in the Lorestan Arc that we set up as part of a previous, more extensive investigation. The purpose of our study was to evaluate the possible role of some "unconventional" controlling factors - whose relevance for large-scale gravitational processes had already been demonstrated - in landslide susceptibility. In the early stage of the study, susceptibility assessment was based on the Frequency Ratio method, a simple but reliable technique, at least for first-level screening. This bivariate statistical method consists of comparing the spatial distribution of landslides with conditioning factors, taken individually, in the study area. The Frequency Ratio, which assesses the relative importance of each factor in landslide processes (Trigila *et alii*, 2015), requires discrete reclassification of continuous variables. The novelty of this study is that it takes into consideration both static factors (slope, aspect, relief, wetness index, and lithology) and pseudo-dynamic elements as potentially triggering elements (distance from active faults and stream steepness index, a proxy of tectonic uplift) in the analysis. In particular, potentially triggering factors were taken to be both time-averaged transient forcing effects and predisposing factors damaging the rock mass over time. Indeed, they combine the effects of transient tectonic forces of individual seismic events and morphotectonic effects on the slope-valley system.

REGIONAL GEOLOGICAL SETTING AND STRATIGRAPHY OF LORESTAN

The Zagros Mountain range is part of the Alpine-Himalayan orogenic system that originates from the Late Cretaceous-Cenozoic convergence between Africa and Arabia-Eurasia (e.g. Mouthereau *et alii*, 2012). The Zagros orogen has been traditionally classified, based on distinctive lithological units and structural styles, into four NW-trending tectono-metamorphic and magmatic belts (Figure 1). The latter are bounded by structural features of a regional scale, such as the Main Zagros Reverse Fault (MZRT), High Zagros Fault (HZF), and Mountain Front Fault (MFF) (Agard *et alii*, 2005, and references therein). These tectonic units are as follows (from the inner to the outer sectors of the belt): 1) the Urumieh Dokhtar volcanic arc, 2) the Sanandaj-Sirjan Zone, 3) the Imbricate Zone, 4) the Zagros (or Simply) folded belt, and 5) the continental Mesopotamian Foreland.

The Lorestan region, on which this study is focused, lies in the latter tectonic domain and extends between the HZF to the NE and the MFF to the SW. The Simply Folded Belt involves, in spectacular folds, the 12–14 km thick sedimentary rocks of the Arabian margin succession covering the continental basement (e.g. McQuarrie, 2004). The irregular geometry of the MFF that bounds the Simply Folded Belt south of the Mesopotamian foreland basin, describes salients and reentrants (McQuarrie, 2004; Sepehr & Cosgrove, 2004): from NW to SE, the Lorestan, the Dezful Embayment, the Izeh Zone, and the Fars Arc, respectively (Figure 1).

In a representative balanced cross-section of the Dezful embayment, Blanc *et alii* (2003) measured a ~49 km of shortening across the Simple Folded Zone. Homke *et alii* (2004) provided dates of 8.1 and 7.2 Ma for the onset of the deformation in the front of the Pusht-e Kuh Arc (related to the base of the growth strata observed on the northeastern side of the Changuleh syncline) that lasted until 2.5 Ma, around the Pliocene–Pleistocene boundary. A long-term shortening rate of ~10 mm y-1 was derived for the deformation in the Simple Folded Zone, which is the same as the present-day one derived from GPS measurements (Tatar *et alii*, 2002). In the Lorestan area, instrumental seismicity (U.S. Geological Survey, 2020) in the 2006-2020 period was distributed over a wide 200-300 km^2 area of the Zagros Mountain range (Hatzfeld *et alii*, 2010; Paul *et alii*, 2010; Rajabi *et alii*, 2011), with a sharp cut from the HZF to the MFF in the NW and SE, MZRF in the NE (e.g. Yamini-Fard *et alii*, 2006), with recurrent earthquakes of Mw 5-6 and exceptional earthquakes of higher magnitude, i.e. of up to Mw 6-8 (Figure 1) indicating that HZF,MFF and BF are still active. The two active areas are associated with transferring zones, which border the Lorestan salient and the Dezful and Kirkuk reentrants.

The 12-14 km thick sedimentary succession is composed of both the passive margin sequence, lasting from the Upper Paleozoic to the Late Cretaceous, as well as of the foreland sequence, occurring from the Late Cretaceous to the present (James & Wynd, 1965; Casciello *et alii*, 2009; Verges *et alii*, 2011). The Mesozoic succession testifies that the region was dominated by large carbonate platforms with associated shallow basins filled with marls, shales, and marly limestones interbedded with episodic plugs of evaporites, typical of a passive margin. It includes the carbonates of the Bangestan Group (Garau, Sarvak, Ilam-Surgah Formations), one of the largest reservoirs of hydrocarbons in Iran, as well as the Gurpi Formation. Afterwards, two clastic wedges developed, separated by the Early-Middle

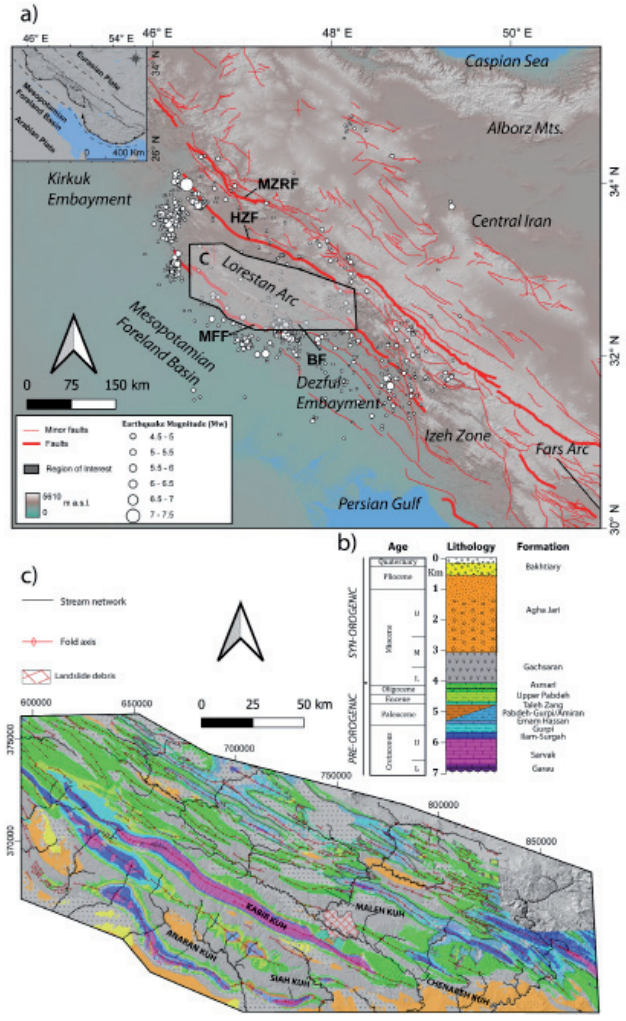

Fig. 1 - a) Regional sketch of the Zagros Mountains, showing the region of interest and the instrumental seismicity (U.S. GEOLOGICAL SURVEY, 2020) of the area in the 2006-2020 period. MFF: Mountain Front Fault, HZF: High Zagros Fault, MZRF: Main Zagros Reverse Fault, BF: Balarud Fault. The coordinate system is WGS84 EPSG: 4326. b) Stratigraphic column and c) geological map of the Lorestan Arc (coordinates are WGS84-38N, EPSG: 32638). The trace and kinematics of the active faults are taken from the GEM Global Active Fault database (STYRON & PAGANI, 2020). The map colour scale indicates elevation, which is derived from the 30 m SRTM (Farr et alii, 2007)

Miocene carbonate of the Asmari Formation (Casciello *et alii*, 2009; Verges *et alii*, 2011): the proto-Zagros foreland sequence (Paleocene-Early Eocene) and the Mesopotamian foreland succession (Miocene-Early Pleistocene).

The proto-Zagros sequence (Emam Hassan Member, Pabdeh-Gurpi, Amiran, Taleh Zang, and Pabdeh Formations) consists of an alternation of contrasting lithotypes, from marls to limestones, while evaporites, sandstones, and conglomerates characterise the foreland succession (Gachsaran, Agha Jari, and Bakhtiari Formations).

Generally, the anticlines in the Simply Folded Belt are well exposed in the resistant Oligo-Miocene limestones of the Asmari Formation and the Cretaceous group of Bangestan, which are often more than 100 km long (Ramsey *et alii*, 2008). The folding mechanisms appear to be influenced by stratigraphy, depth, and regional tectonic setting (Burberry *et alii*, 2008, 2010).

In this regard, the drainage network adapted to the growth of the thrust-fold structures (Ramsey *et alii*, 2008) and to the erodibility of the outcropping formations (Oberlander, 1985). Oberlander (1968) suggested that the drainage network in the NW Zagros was superimposed on structurally conformable younger horizons. In his model, the breaking of hard geological units of the antiformal ridges followed a phase of river cutting and expansion of the fold axial basins through the softer overlying units. On Oberlander's (1968) assumption, it was the Pabdeh and Gurpi marls that facilitated the creation of a low-relief landscape across the anticline crests, thus contributing to landscape shaping.

MATERIALS AND METHODS

Landslide Inventory

Landslide susceptibility was assessed on the basis of an unprecedented inventory of landslides in the Lorestan Arc.

The inventory was built by relying on the Google Earth satellite imagery (2019 Landsat Imagery) and on the geological maps provided by the National Iranian Oil Company (NIOC) at a scale of 1:100,000 (Figure 2). In particular, use was made of the following sheets: Balarud (Sahabi & Macleod, 1969), Dalpari (Setudehnia & O'b Perry, 1977), Dehluran (Llewellyn, 1973), Kabir-kuh (Macleod, 1970), Khorramabad (Fakhari, 1985), Kuh-e-Anaran (Setudehnia, 1967), Kuh-e-Varzarin (Macleod & Roohi, 1970), Mehran (Macleod & Roohi, 1972), Naft (Macleod & Fozoonmayeh, 1971), Pul and Dukthar (Takin & Macleod, 1970), and Palganeh (Llewellyn, 1974).

We classified gravitational movements according to the classification of Hungr *et alii* (2014), distinguishing: 55 rock avalanches, 16 ongoing mass rock creep deformations, 10 flexural topplings, 323 "Falls", 34 flows, 297 "Slides", and 11 lateral spreads (Figure 2). Based on similarities in terms of kinematic and failure mechanisms, the "Falls" category includes both "Falls" and topples, while "Slides" include both rotational and translational movements. In particular, to evaluate the conditioning factors for the above-mentioned movements, we mapped only the detachment area or deforming zone in a GIS environment. Susceptibility analysis was carried out only on the "Falls" and "Slides" categories, the numbers of which were considered to be statistically robust, unlike those of other categories (Figure 2).

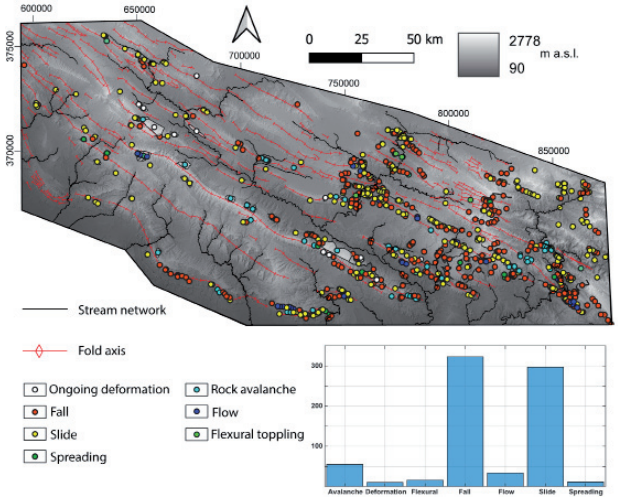

Fig. 2 - Landslide inventory map of the Lorestan Arc, showing the train and test movement datasets (1 and 2, respectively) and the landslide category histograms (coordinates are WGS84-38N, EPSG: 32638). The map colour scale indicates elevation, which is derived from the 30-m SRTM (Farr et alii, 2007)

Susceptibility Analysis

Susceptibility was assessed by applying the Frequency Ratio method. The computation was carried out on the Shuttle Radar Topography Mission (SRTM, Farr *et alii*, 2007) Digital Elevation Model (DEM) provided by NASA JPL at a resolution of 1 arc-second (30 m).

Frequency Ratio is a quantitative technique for landslide susceptibility assessment using GIS techniques and spatial data (e.g. Bonham-Carter, 1994, and Lee & Talib, 2005). It is based on a quantified association between the landslide inventory and conditioning factors (including static and pseudo-dynamic or triggering elements) (e.g. Reis *et alii*, 2012). To obtain the Frequency Ratio (*FR*) for each class of conditioning factors, a combination was established between the landslide inventory map and each factor map using Eq. (1) (e.g. Mondal & Maiti, 2013). Let L and F stand for a landslide and a certain landslide-related factor, respectively. Given that the factor *F* is categorised into n types or subdivided into n classes, the frequency ratio (*FR*) for the ith type or the ith class of factor *F* (*Fi*) can be written as:

$$FR_i = \frac{PL_i}{PF_i} = \frac{the\ landslide\ frequency\ in\ the\ F_i\ area}{the\ F_i\ area\ frequency} = \frac{\frac{the\ landslide\ area\ in\ the\ F_i\ area}{the\ landslide\ area\ in\ the\ study\ area}}{\frac{the\ F_i\ area}{the\ study\ area}} \quad (1)$$

A

frequency ratio *FRi* above 1 indicates that "the landslide frequency or probability in the Fi area" (*PLi*) is larger than "the Fi area frequency or probability" (*PFi*) and further indicates that the ith type or the ith class of factor *F* (*Fi)* promotes the occurrence of land"Slides". On the contrary, a frequency ratio *FRi* below 1 indicates that Fi does not promote the occurrence of land"Slides".

Consider an arbitrary landslide-related factor *F(j) (j = 1, 2, 3, ..., m)*; its frequency ratios regarding different types or classes, namely *FRi (j) (i = 1, 2, 3, ..., n; j = 1, 2, 3, ..., m)*, can be calculated according to Eq. (1). If the type or class of *F(j)* at a certain location is *Fi (j)*, the frequency ratio of this factor at this location *FR(j)* will be *FRi (j)*. Thus, the landslide susceptibility index (LSI) at this location will be the summation of the frequency ratios of different landslide-related factors at this location (e.g. Lee & Pradhan, 2007):

$$LSI = \sum_{j=1}^{m} FR^{(j)} \quad (2)$$

The resulting susceptibility scale unit is 30 m pixel sized.

The conditioning factors considered in the FR analysis were distinguished into static and pseudo-dynamic.

Static factors included:

- slope angle (°) - steepest downward numerical gradient of a DEM using an 8-connected neighbourhood;
- aspect (°) - slope direction of each cell in a DEM;
- relief (m) – local topography, such as the elevation range within a specific radius (5000 m);
- topographic Wetness Index (TWI) – predictor of potential soil moisture and, thus, of sensitivity to hydraulic triggers. It is defined by the following equation:

$$TWI = ln\left(\frac{A}{tan\ (\beta)}\right) \quad (3)$$

- where *A* is the contributing upslope area and tanβ is the local slope (Moore *et alii*, 1991);
- lithology-lithological units obtained from the geological map of Iran 1:100,000.

We considered pseudo-dynamic factors as a proxy of tectonic activity cumulating the effects of the transient triggering forces of individual tectonic events, including:

- distance from Active Faults-DAF (m) – orthogonal distance to the nearest faults. This index is also an indirect measure of the damage of rock masses, which is expected to be more intense in the proximity of a fault and to decrease with distance. The trace and kinematics of the active faults were taken from the GEM Global Active Fault database (Styron & Pagani, 2020).
- steepness index (ksn) – channel steepness index, a measure of channel gradient normalised for downstream increases of

the drainage area that is a proxy of regional tectonic uplift.

Under the Stream Power Law (SPL) approach, the evolution of a river profile is described as the change in elevation z of a channel point x through time t (Howard & Kerby, 1983), which relates to the competition between erosion (*E*) and uplift (*U)*:

$$\frac{dz(x,t)}{dt} = U(x,t) - E\,(x,t) \tag{4}$$

In a steady-state condition, the difference between *E* and *U* is equal to 0 and the fluvial erosion *E* or uplift *U* is computed as:

$$E\,(x,t) = K\,A\,(x)^{\,m}\left(\frac{dz\,(x,t)}{dx}\right)^{n} \tag{5}$$

The powers m and n are positive constants controlling the erosion mechanism. Specifically, m depends on the climatic conditions and hydraulic properties of discharge, and n is a function of other erosional thresholds (Whipple & Tucker, 1999; Di Biase & Whipple, 2011). The erodibility, *K*, accounts for lithology, climatic conditions, and channel geometry. In general, *K* may change in space and time, but here it is taken as a constant.

A power-law relationship between the local channel slope (*S*) and the upstream drainage area (A) reveals the steady-state river profile:

$$S\,(x,t) = \left(\frac{U(x,t)\ or\ E(x,t)}{K}\right)^{\frac{1}{n}} A(x)^{-\frac{m}{n}} \tag{6}$$

and

$$k_{sn} = \left(\frac{U(x,t)\ or\ E(x,t)}{K}\right)^{\frac{1}{n}} \tag{7}$$

where *ksn* is known as the steepness index, and the *m/n* ratio or θ is defined as a concavity index.

The computation of the steepness index was carried out along river profiles and extracted by setting a flow accumulation threshold according to that proposed for the fluvial domain (10^{-1} km^2) by Montgomery & Foufoula-Georgiu (1993) with MATLAB using the Topo Toolbox suite of functions (Schwanghart & Scherler, 2014). The steepness index was computed at the outcropping area of the carbonate carapace belonging to the Bangestan Group and the Asmari Formation. In this way, the signal recorded by the ksn with the same lithology can be considered as a direct proxy of tectonic uplift. Mapping interpolation was performed with the Inverse Weighted Distance (IWD) algorithm in a GIS environment.

Before passing to susceptibility analysis proper, we first explored the existence of a significant relation between the two pseudo-dynamic factors and the presence/absence of landslides. For this purpose, we analysed the results of a univariate logistic regression performed by randomly sampling, for each type of instability, the ksn and DAF values at 2774 and 2529 stable points (i.e. located within landslide polygons) for "Falls" and "Slides", respectively, and 3407 unstable points (assuming the values "0" and "1", respectively) for both types of landslide, the latter being located at a sufficient distance from landslide areas. The logistic regression used the open access software JASP 0.14.1 (JASP Team, 2020).

Validation Analysis

As a diagnostic test for evaluating accuracy of the susceptibility model and significance of the selected pseudo-dynamic factors for each type of landslide, the complete dataset of source areas was randomly split in two subsets, containing 80% and 20% of the original dataset, respectively. After checking the consistency of the two subsets in terms of distribution of the values of variables (Figures 3 and 4), the larger one was used to train the susceptibility function and the smaller one for validation purposes. In particular, we sampled the predicted susceptibility values in the location of the actual landslides contained in the validation. This allowed us to generate prediction rate curves where the portion of areas predicted as a hazard was plotted against the portion of the actually occurred landslide (Chung & Fabbri, 2003). Prediction accuracy is generally measured by the Area Under the Curve (AUC). The prediction rate provides a validation of the prediction regardless of the prediction model used.

RESULTS

Multi-parametric analysis and delineation of variable classes

Susceptibility analysis was initially based on a multi-parametric statistical approach, considering dependent variables or landslide classes susceptible to independent variables, e.g. the conditioning factors mentioned in the previous section.

Figure 3 shows the box plots of all the pixels belonging to the "Falls" and "Slides" for slope angle, relief, distance from active faults, ksn, and TWI factors, as well as the rose plot of all the pixels belonging to the "Falls" and "Slides" areas for the aspect factor. In each box, the central mark indicates the median, whereas the bottom and top edges of the box indicate the 25th and 75th percentiles, respectively. The pie plots in Figure 4 show the fraction of the entire landslide ("Falls" and "Slides") area falling under each category of lithology. With a view to classifying continuous variables (as required by the Frequency Ratio method), we first analysed the value distribution in the landslide source areas for each variable (and separately for each type of landslide).

The multi-parametric analysis enabled us to define the thresholds necessary for reclassifying each factor. In this regard, we decided to define three classes, equally spaced between the

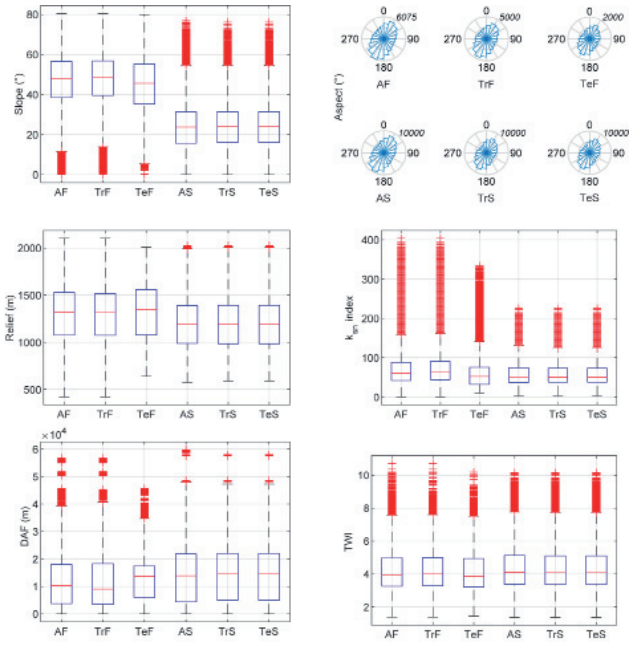

Fig. 3 - Box plots of all the pixels belonging to all "Falls" and "Slides" areas (AF-All "Falls"; AS-All "Slides"), training "Falls" and "Slides" areas (TrF-Training "Falls"; TrS-Training "Slides"), and test "Falls", and "Slides" areas (TeF-Test "Falls"; TeS-Test "Slides") are shown for slope, relief, DAF (Distance from Active Fault), ksn, and TWI (Topographic Wetness Index) factors. The rose plot is shown for the aspect factor

25th and 75th quantiles, alternatively the 2nd and 3rd quartiles (edges of the box), another two for the 1st and 4th quartiles, and, if necessary, another one covering the outlier range values. Then, to ensure a correct application of the results of the training to the test datasets, we checked the mutual consistency of the randomly split datasets in terms of similarity of distribution of the values of variables. A comparison of the boxplots, bar diagrams, and rosette plots of Figures 3 and 4 (for continuous, categorical, and circular-scale variables, respectively) shows a good consistency between the training and test datasets.

With regard to slope angle values, the distribution for "Falls" is concentrated between 38° and 60°, while that for "Slides" shows a lower value range between 18° and 35°. Conversely, the aspect values show a strong correspondence between the distributions of each type of instability, and they are concentrated towards SW and NE. The aspect classes were delineated as follows: 1) flat surfaces; 2) 0°-22.5° N; 3) 22.5°-67.5° N; 4) 67.5°-112.5° N; 5) 112.4°-157.5° N; 6) 157.5°-202.5° N; 7) 202.5°-247.5° N; 8) 247.5°-292.5° N; 9) 292.5°-337.5° N; 337.5°-360° N. As for relief energy (with a 5000 m radius), its values are generally higher for "Falls" (1100-1550 m) than for "Slides" (1000-1400 m). The steepness index distribution shows a significant presence of outliers in all the classes that can be connected with unbalanced values of the DEM along the drainage courses, especially near gorges. The values of "Falls" appear to be slightly higher than those of "Slides". In general, most of the values of the types of instability are lower than 100. The Distance from Active Fault (DAF) factor also shows a similarity between the median values relating to all types of landslide. Generally, the distance is around 10 km for "Falls" and 15 km for "Slides", especially near the MFF, HZF, and BF. As regards the TWI, the median values for all the types of landslide range between 3 and 5. Finally, the lithological factor (Figure 4) highlights that the lithotypes most involved in "Falls" and "Slides" are limestones (>50% for both categories) and marly limestones (10-25% for both categories). For "Falls", also the fraction of calcirudites and marls (10-15%) is considerable.

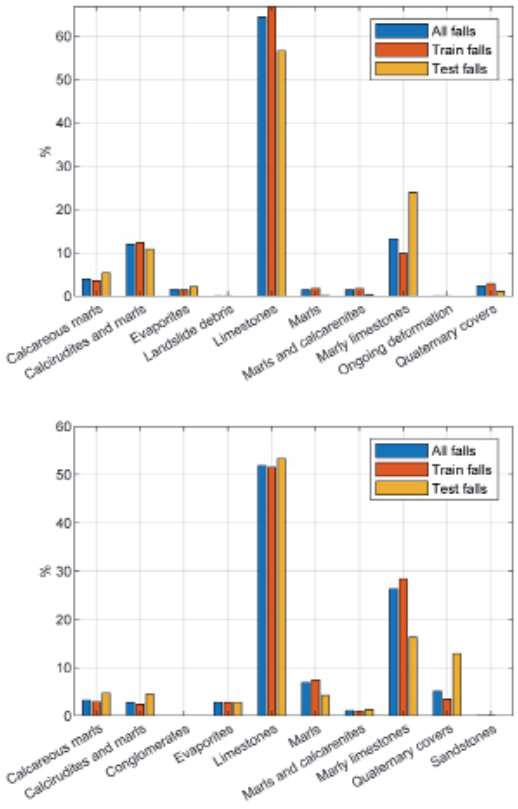

Fig. 4 – Bar plots for "Falls" (a) and "Slides" (b) of all the pixels belonging to all landslides; training and test areas are shown for each category of lithology

Susceptibility models

Figure 5 presents the model summary and the performance diagnostics of the univariate logistic regression between the pseudo-dynamic factors and a randomly generated set of "stable"

Model Summary

a) DAF - Falls

Model	Deviance	AIC	BIC	df	X^2	p	McFadden R^2	Nagelkerke R^2	Tjur R^2	Cox & Snell R^2
H_0	8503.746	8505.746	8512.475	6180						
H_1	8329.061	8333.061	8346.519	6179	174.685	< .001	0.021	0.028	0.027	0.028

b) Steepness index (k_{sn}) - Falls

Model	Deviance	AIC	BIC	df	X^2	p	McFadden R^2	Nagelkerke R^2	Tjur R^2	Cox & Snell R^2
H_0	8503.746	8505.746	8512.475	6180						
H_1	7227.232	7231.232	7244.690	6179	1276.514	< .001	0.150	0.187	0.193	0.187

c) DAF - Slides

Model	Deviance	AIC	BIC	df	X^2	p	McFadden R^2	Nagelkerke R^2	Tjur R^2	Cox & Snell R^2
H_0	8098.700	8100.700	8107.388	5935						
H_1	8027.042	8031.042	8044.419	5934	71.658	< .001	0.009	0.012	0.012	0.012

d) Steepness index (k_{sn}) - Slides

Model	Deviance	AIC	BIC	df	X^2	p	McFadden R^2	Nagelkerke R^2	Tjur R^2	Cox & Snell R^2
H_0	8098.700	8100.700	8107.388	5935						
H_1	7410.860	7414.860	7428.238	5934	687.839	< .001	0.085	0.109	0.115	0.109

Performance Diagnostics

e)

Confusion matrix

Observed	Predicted 0	Predicted 1
0	2369	1038
1	1604	1170

Performance metrics

	Value
AUC	0.589

f)

Observed	Predicted 0	Predicted 1
0	2819	588
1	1347	1427

	Value
AUC	0.775

g)

Observed	Predicted 0	Predicted 1
0	3407	0
1	2529	0

	Value
AUC	0.562

h)

Observed	Predicted 0	Predicted 1
0	2832	575
1	1469	1060

	Value
AUC	0.729

Fig. 5 – Model summary (a, b, c, and d) and performance diagnostics (e, f, g, and h) - including confusion matrix and performance metrics (AUC) - of the univariate logistic regression of the DAF factor for "Falls" landslides (a and e), steepness index factor for "Falls" landslides (b and f), DAF for "Slides" landslides (c and g), and steepness index factor for "Slides" landslides (d and h). The analysis was carried out by using the open access software JASP 0.14.1 (JASP Team, 2020) on a randomly generated set of "stable" (0) and "unstable" (1) points

(0) and "unstable" (1) points. The model statistics, reported in the summary (Figure 5 a, b, c, and d), demonstrate the statistical significance of the relationship between pseudo-dynamic factors and landslide presence or absence.

Moreover, the confusion matrix indicates that the steepness index is a good discriminatory factor for both "stable" and "unstable" points, in contrast to the Distance from Active Fault. However, the AUC metric related to the factors highlights the significance of the pseudo-dynamic factors in landslide occurrence. These results are regarded as exploratory of the statistical significance of pseudo-dynamic variables.

To compute the landslide susceptibility index (LSI) by summing the frequency ratios of each conditioning factor and using Eq. (1), we first reclassified (in a GIS environment) the independent variables according to the quartile distributions obtained from the multi-parametric analysis of the test dataset of each type of landslide.

By combining the reclassified layers with the dependent variables, such as "Falls" and "Slides" training categories, a unique output value was assigned to each unique combination of input values. The frequency ratio was therefore calculated for each class of each factor; subsequently, we reclassified the previously identified classes based on the frequency ratio values obtained (Figure 6). By calculating the frequency ratios for each

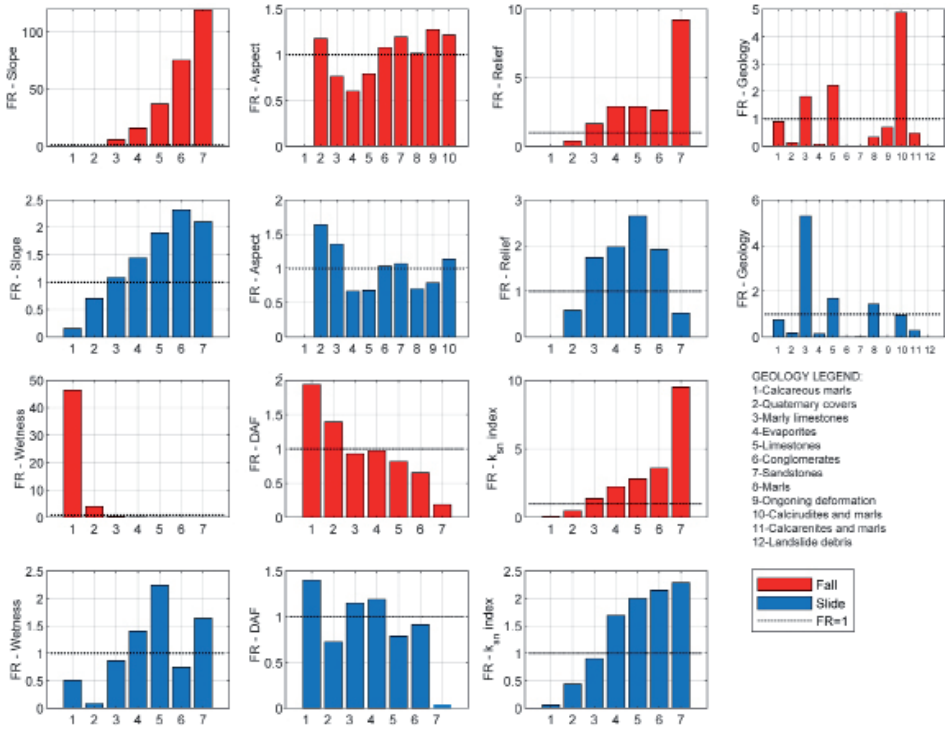

Fig. 6 – Bar plots of the partial frequency ratios distinguished by classes relative to each factor for "Falls" and "Slides". The classes were delineated by using the distribution of variables shown in Figure 3 (detailed procedure described in the text). The frequency ratio line equal to 1 is plotted on all the bar plots to indicate the importance of each class in landslide susceptibility. The geology legend is included

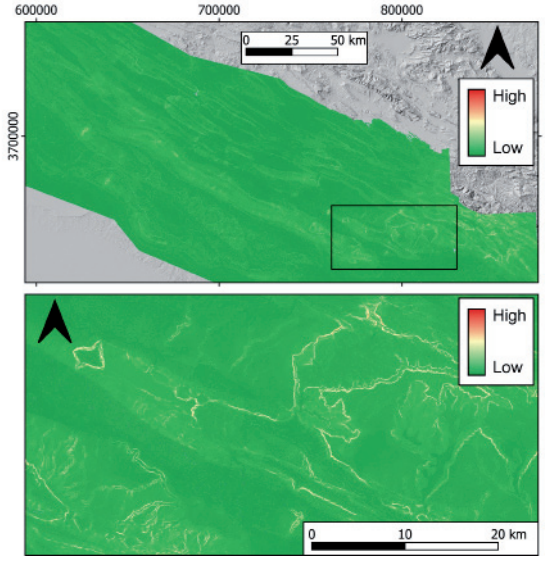

Fig. 7 - "Falls" susceptibility map based on frequency ratios (coordinates are WGS84-38N, EPSG: 32638) and enlargement of an example area to better observe the result

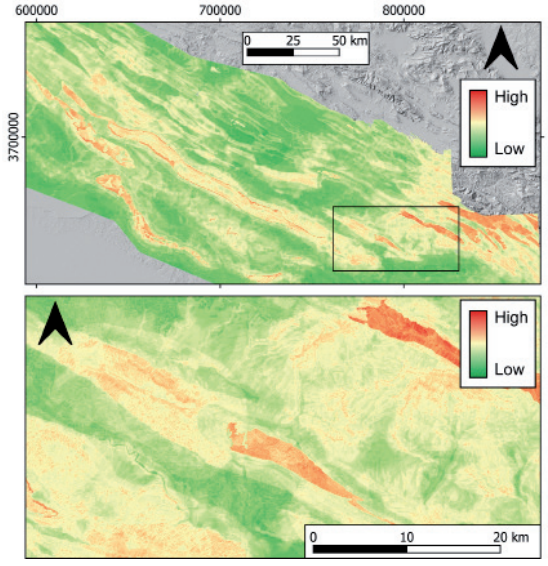

Fig. 8 – Landslide susceptibility map based on frequency ratios (coordinates are WGS84-38N, EPSG: 32638) and enlargement of an example area to better observe the result

class of investigated variable, we could assess the importance of the variables on a preliminary basis.

Indeed, Figure 6 shows the frequency ratio line to be equal to 1, indicating the importance of each class in landslide susceptibility. Slope and TWI appear to be crucial elements in terms of susceptibility to "Falls", whereas "Geology" plays a decisive role in susceptibility to "Slides".

The susceptibility maps (Figures 7 and 8) are the result of the summation of the frequency ratios of each conditioning factor using Eq. (1).

In more detail, Figure 7 shows the susceptibility map obtained for the "Falls" type of landslide. The model highlights very well that areas with slope angles greater than 40° are prone to detachment. These areas are associated with both high relief energy and low TWI values while, from a tectonic point of view, susceptibility increases with increasing ksn and decreasing fault distance. In this sense, triggering elements appear to play a very significant role in the development of this kind of instability. As can be seen in the bottom part of Figure 8, susceptible areas are associated with outcrops of the most resistant lithotypes, such as limestone and marly limestone belonging to the Bangestan Group and Asmari Formation. Specifically, the "Falls" instabilities are associated very well with the creation of landforms, such as tangs, wind gaps, and water gaps by the drainage network. The top part of Figure 8, in contrast, shows the susceptibility map relating to the landslide class.

The maps show that highly susceptible areas are those having slope values of 20° to 35°, outcrops of the most resistant lithotypes - e.g. limestone and marly limestone belonging to the Asmari and Pabdeh Formations and the Bangestan Group -, and low TWI values. Erosional morphologies, such as flatirons, are highlighted as very susceptible to slide detachment. Furthermore, local relief plays an active role in landslide predisposition, showing higher frequency ratios in association with value classes between 1000 m and 1500 m. From a tectonic point of view, in this instance, too, susceptibility increases with increasing ksn and decreasing fault distance.

To assess the importance of variables more carefully, we decided to use our actual units of analysis (i.e. landslide polygons) rather than the prediction rate curve, which is based on mapping units (i.e. pixel by pixel), regardless of the uniqueness of landslide scars. In particular, we computed the mean LSI value within each source area and compared it with the mean FR value of each variable in the same area, thus quantifying the actual contribution of controlling factors from another perspective. As shown in Table 1, the most significant contribution of conditioning variables in determining the mean LSI is given by slope (70.04%) and TWI (8.59%) for "Falls" and by lithology (20.94%) and slope (18.27%) for "Slides".

	SLOPE	ASPECT	RELIEF	k_{sn}	DAF	TWI	LITHOLOGY
FALLS	70.04%	2.67 %	4.31 %	5.71%	2.93%	8.59%	5.76 %
SLIDES	18.27%	12.18 %	13.83 %	15.59%	10.79%	8.30%	20.94 %

Tab. 1 – Contribution of the factors in determining the mean landslide susceptibility index value in actual landslides for both types of landslide

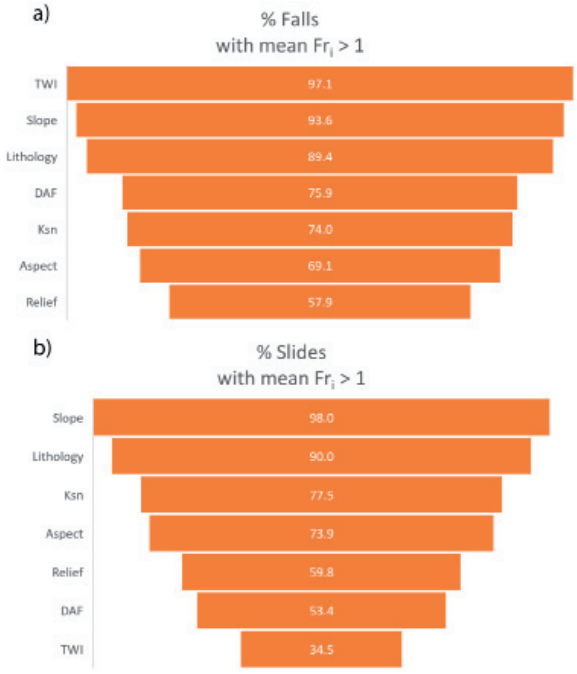

Fig. 9 – Funnel charts for "Falls" (a) and "Slides" (b) with percentages of landslides in which the frequency ratio relative to each variable was above 1, evidencing the importance of variables in landslide susceptibility

In Figure 9 the percentage of landslide cases in which the frequency ratio relative to each conditioning factor is greater than 1, is reported. In "Falls" category, frequency ratios of TWI, slope and lithology are greater than 1 in the 97.1%, 93.6% and 89.4% of the landslide cases, while in "Slides", the most important conditioning factors are slope and lithology whose frequency ratio is greater than 1 in 98% and 90% of the cases, respectively.

Validation results

Landslide susceptibility analysis results were tested using a dataset test sample of the 65 "Falls" and 59 "Slides" resulting from the random splitting of the original dataset into train (80%) and test (20%) subsets.

Validation results are shown in Figure 10 for both "Falls" and "Slides". The prediction rate curve, based on the classification of the LSI into 10 classes according to Jenks' natural breaks criterion, shows a very good performance for "Falls" (AUC = 0.94) and a satisfactory outcome for "Slides" (AUC = 0.77). The better performance for "Falls" than for "Slides" can be attributed to the intrinsic nature of the process and the related sensitivity to a narrower range of parameters (especially lithology and slope), as well as to potential incompleteness of the inventory.

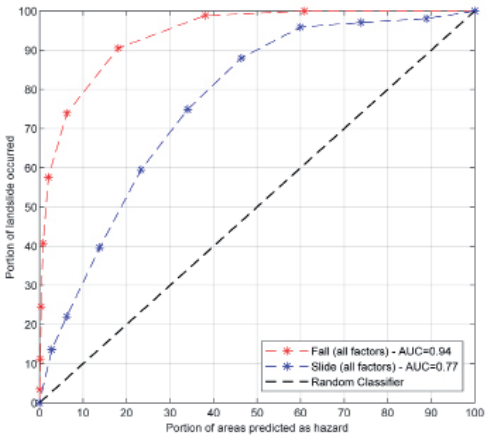

Fig. 10 – Prediction rate curves of "Falls" and "Slides" susceptibility models

CONCLUDING REMARKS

Landslides represent one of the most impacting natural hazards worldwide, and their assessment has often been attempted over the years via statistical susceptibility analyses (Reichenbach *et alii*, 2018). This paper deals with the preliminary results of a bivariate susceptibility analysis, which was carried out on two landslide classes deriving from an unpublished inventory for the Lorestan region (Zagros Mountains, Iran): "Falls" (323 cases) and "Slides" (297 cases). In particular, use was made of the Frequency Ratio (FR) method, which consists of combining the spatial distribution of landslides with conditioning factors (Trigila *et alii*, 2015). Among more traditional morphological (slope, aspect, relief), hydraulic (TWI), and geological (fault distance, lithology) factors, we introduced pseudo-dynamic factors. We regarded the latter as potentially triggering factors over the medium-long term and thus combining both the effects of the transient tectonic forces arising from individual seismic events and morphotectonic effects on the slope-valley system. In this new class of factors, we tested a new tectonic and structural factor, which was interpolated with an IDW algorithm obtained from a map of the steepness index ksn of longitudinal stream profiles (Whipple & Tucker, 1999; Di Biase & Whipple, 2011). As shown in Eq. (7), this index, which can be appropriately isolated from the lithological influence of the erodibility K (exposure of resistant Oligo-Miocene limestones belonging to the Asmari Formation and the Cretaceous group of Bangestan along the anticlines of the arc), can be considered as a direct proxy of tectonic uplift. Univariate logistic regression applied to pseudo-dynamic factors (Distance from Active Fault and steepness index) demonstrated their statistical significance.

Susceptibility models were built for 261 "Falls" and 237 "Slides". They were then tested by using a dataset test sample of the 65 "Falls" and 59 "Slides" resulting from the random splitting

of the original dataset into train (80%) and test (20%) subsets.

With a view to classifying continuous variables (as required by the Frequency Ratio method), we initially analysed the distribution of values in the landslide source areas for each variable (and separately for each type of landslide). A multi-parametric analysis enabled us to define the thresholds necessary for reclassifying each factor. Moreover, to ensure a correct application of training results to the test datasets, we checked the mutual consistency of the randomly split datasets in terms of similarity of distribution of the values of variables.

In the Lorestan region, there exist similar environmental, morphological, and geological factors for both kinds of gravitational instability:

- contrasting rheological behaviour in terms of stratigraphy (limestones, marly limestones, marls; calcirudites and marls);
- moderate to high slope angle (between 18° and 35° for "Slides", and between 38° and 60° for "Falls");
- high relief energy ("Falls" around 1100-1550 m and "Slides" 1000-1400 m);
- the aspect variable highlights that slopes are dominantly SW- and NE-oriented, which suggests a possible correlation with the tectonic direction of the Zagros belt (SW vergence);
- low *TWI* values indicate areas with low flow accumulation and high slopes characterised by low potential soil moisture.

The analysis of the sensitivity of landslide classes to pseudo-dynamic or potentially triggering and structural factors inferred a strong correlation between the occurrence of gravitational movements and the activity and distance of the main active tectonic features (MFF, BF, HZ). In particular, for both landslide classes:

- the median distance from the active fault is 10 km for "Falls" and 15 km for "Slides", in the proximity of the MFF, HZF, and BF;
- the median ksn values lie between 50 and 100; ksn values were only recorded above the outcropping carbonate carapace belonging to the Bangestan Group and the Asmari Formation, indicating that (in the absence of lithological control) the highest ksn values correspond to the most uplifted areas along the main fold structures of the Lorestan Arc, especially in the southeastern zone.

The validation of the prediction rate curve for our susceptibility models yielded a landslide prediction accuracy of 94% and 77% for "Falls" and "Slides", respectively. The better performance for "Falls" than for "Slides" can be ascribed to the intrinsic nature of the process and the related sensitivity to a narrower range of parameters (especially lithology and slope), as well as to potential incompleteness of the inventory.

To assess the importance of variables more carefully, we computed the contribution of conditioning factors in determining the mean landslide susceptibility index value in actual landslides, as well as the percentage of landslide cases in which the frequency ratio relative to each variable was above 1. This process indicated that the most important factors were *TWI*, slope and lithology for "Falls", and slope and lithology for "Slides". In spite of this, the *DAF* and ksn showed a significant correlation with landslides. If the former is a proxy of both inherited rock mass damage and severity of seismic shaking (thus difficult to be univocally interpreted), the latter is a more unconventional parameter that has a precise meaning and contributes to landslide proneness significantly. This evidence stresses the importance of morphostructural evolution and the need for placing landslide processes within a temporally wider morphoevolutionary framework.

The study covered by this paper also represents one of the first bivariate susceptibility analyses conducted in Lorestan, where the Seymareh rock avalanche, the largest subaerial landslide in the world, occurred (Roberts & Evans, 2013; Rouhi *et alii*, 2019; Delchiaro *et alii* 2019 a, b, 2020a).

REFERENCES

Agard P., Omrani J., Jolivet L. & Mouthereau F. (2005) - *Convergence history across Zagros (Iran): constraints from collisional and earlier deformation*. International Journal of Earth Sciences, **94** (3): 401-419.

Agliardi F., Zanchi A. & Crosta G. B. (2009) - *Tectonic vs. gravitational morphostructures in the central Eastern Alps (Italy): constraints on the recent evolution of the mountain range*. Tectonophysics, **474** (1-2): 250-270.

Blanc E. P., Allen M. B., Inger S. & Hassani H. (2003). *Structural styles in the Zagros simple folded zone, Iran.* Journal of the Geological Society, **160** (3): 401-412.

Bohnam-Carter G. F. (1994) - *Geographic information systems for geoscientists-modeling with GIS. Computer methods in the geosciences,* **13**: 398 pp.

Burberry C. M., Cosgrove J. W. & Liu J. G. (2008) - *Spatial arrangement of fold types in the Zagros Simply Folded Belt, Iran, indicated by landform morphology and drainage pattern characteristics*. Journal of Maps, **4** (1): 417-430.

Burberry C. M., Cosgrove J. W. & Liu J. G. (2010) - *A study of fold characteristics and deformation style using the evolution of the land surface: Zagros Simply Folded Belt, Iran.* Geological Society, London, Special Publications, **330** (1): 139-154.

Casciello E., Verges J., Saura E., Casini G., Fernandez N., Blanc E., Homke S. & Hunt D. W. (2009) - *Fold patterns and multilayer*

rheology of the Lurestan Province, Zagros simply folded belt (Iran). Journal of the Geological Society, **166** (5): 947-959.

Cascini L. (2008) - *Applicability of landslide susceptibility and hazard zoning at different scales.* Engineering Geology, **102** (3-4): 164-177.

Chung C. J. F. & Fabbri A. G. (2003) - *Validation of spatial prediction models for landslide hazard mapping*. Natural Hazards, **30** (3):451-472.

Delchiaro M., Della Seta M., Martino S., Dehbozorgi M. & Nozaem R. (2019a) - *Reconstruction of river valley evolution before and after the emplacement of the giant Seymareh rock avalanche (Zagros Mts., Iran).* Earth Surface Dynamics, **7** (4): 929-947.

Delchiaro M., Rouhi J., Della Seta M., Martino M., Dehbozorgi M. & Nozaem R. (2019b) - *Geostructural and geomorphic constraints for landscape evolution modeling and stress-strain numerical analysis of the giant Seymareh landslide (Zagros Mts., Iran).* Proceedings of the 2019 EGU General Assembly. 7-12 April 2019, Wien, Austria.

Delchiaro M., Rouhi J., Della Seta M., Martino M., Dehbozorgi M. & Nozaem R. (2020a) - *The Giant Seymareh Landslide (Zagros Mts., Iran): A Lesson for Evaluating Multi-temporal Hazard Scenarios.* In Applied Geology. Springer, Cham: 209-225.

Delchiaro M., Mele E., Della Seta M., Martino S., Mazzanti P. & Esposito C. (2020b) - *Quantitative Investigation of a Mass Rock Creep Deforming Slope Through A-Din SAR and Geomorphometry.* In Workshop on World Landslide Forum. Springer, Cham: 165-170.

Di Biase R. A. & Whipple K. X. (2011) - *The influence of erosion thresholds and runoff variability on the relationships among topography, climate, and erosion rate*. Journal of Geophysical Research: Earth Surface, **116** (F4).

Fakhari A. (1985) - *Khorramabad. 1:100 000 Geological Map*. Iran Oil Operating Companies, Geological Exploration Division, Tehran, Iran.

Farr T. G., Rosen P. A., Caro E., Crippen R., Duren R., Hwnsley S., ... & Alsdorf D. (2007) - *The shuttle radar topography mission.* Reviews of geophysics, **45** (2).

Guzzetti F., Carrara A., Cardinali, M. & Reichenbach P. (1999) - *Landslide hazard evaluation: a review of current techniques and their application in a multi-scale study, Central Italy.* Geomorphology, **31**(1-4): 181-216.

Guzzetti F., Galli M., Reichenbach P., Ardizzone F. & Cardinali M. J. N. H. (2006) - *Landslide hazard assessment in the Collazzone area, Umbria, Central Italy.* Natural Hazards and Earth System Sciences, **6** (1): 115-131.

Hatzfeld D., Authemayou C., Van Der Beek P., Bellier O., Lave J., Oveisi B., Tatar M., Tavakoli F., Walpersdorf A. & Yamini-Fard F. (2010) - *The kinematics of the Zagros mountains (Iran).* Geological Society, London, Special Publications, **330** (1): 19-42.

Homke S., Verges J., Garces M., Emami H. & Karpuz R. (2004) - *Magnetostratigraphy of Miocene–Pliocene Zagros foreland deposits in the front of the Push-e Kush arc (Lurestan Province, Iran).* Earth and Planetary Science Letters, **225** (3-4): 397-410.

Howard A. D. & Kerby G. (1983) - *Channel changes in badlands*. Geological Society of America Bulletin, **94** (6): 739-752.

Hungr O., Leroueil S. & Picarelli L. (2014) - *The Varnes classification of landslide types, an update*. Landslides, **11** (2): 167-194.

Hussin H. Y., Zumpano V., Reichenbach P., Sterlacchini S., Micu M., Van Westen C. & Balteanu D. (2016) - *Different landslide sampling strategies in a grid-based bi-variate statistical susceptibility model*. Geomorphology, **253**: 508-523.

Korup O., Densmore A. L. & Schlunegger F. (2010) - *The role of landslide in mountain range evolution.* Geomorphology, **120** (1-2): 77-90.

McQuarrie N. (2004) - *Crustal scale geometry of the Zagros fold-thrust belt, Iran*. Journal of Structural Geology, **26**: 519–535.

James G. A. & Wynd J. G. (1965) - *Stratigraphic nomenclature of Iranian oil consortium agreement area*. AAPG bulletin, **49** (12), 2182-2245.

JASP Team. (2020) - JASP (Version 0.14.1)[Computer software]. Retrieved from https://jasp-stats.org/

Lee S. & Pradhan B. (2007) - *Landslide hazard mapping at Selangor, Malaysia using frequency ratio and logistic regression models.* Landslides, **4** (1): 33-41.

Lee S. & Talib J. A. (2005) - *Probabilistic landslide susceptibility and factor effect analysis*. Environmental Geology, **47** (7): 982-990.

Llewellyn P. G. (1973) - *Dehluran. 1:100 000 Geological Map*. Iran Oil Operating Companies, Geological Exploration Division, Tehran, Iran.

Llewellyn P. G. (1974) - *Palganeh. 1:100 000 Geological Map*. Iran Oil Operating Companies, Geological Exploration Division, Tehran, Iran.

MacLeod J. H. (1970) - *Kabir kuh. 1:100 000 Geological Map.* Iran Oil Operating Companies, Geological Exploration Division, Tehran, Iran.

Macleod J. H. & Fozoonmayh M. (1971) - *Naft. 1:100 000 Geological Map*. Iran Oil Operating Companies, Geological Exploration Division, Tehran, Iran.

Macleod, J. H., & Roohi, M. (1970). *Kuh-e Varzarin. 1:100 000 Geological Map*. Iran Oil Operating Companies, Geological Exploration Division, Tehran, Iran.

Macleod, J. H., & Roohi, M. (1972). *Mehran. 1:100 000 Geological Map*. Iran Oil Operating Companies, Geological Exploration Division, Tehran, Iran.

Mergili, M., Marchesini, I., Alvioli, M., Metz, M., Schneider-Muntau, B., Rossi, M., & Guzzetti, F. (2014) - *A strategy for GIS-based 3-D slope stability modelling over large areas.* Geoscientific Model Development, 7 (6): 2969-2982.

Mersha T. & Meten M. (2020) - *GIS-based landslide susceptibility mapping and assessment using bivariate statistical methods in Simada*

area, northwestern Ethiopia. Geoenvironmental Disasters, **7** (1): 1-22.

Mondal S., & Maiti R. (2013) - *Integrating the analytical hierarchy process (AHP) and the frequency ratio (FR) model in landslide susceptibility mapping of Shiv-khola watershed, Darjeeling Himalaya*. International Journal of Disaster Risk Science, **4** (4): 200-212.

Montgomery D. R. & Foufoula-Georgiu E. (1993) - *Channel network source representation using digital elevation model*. Water Resources Research, **29**: 3925-3934.

Mouthereau F., Lacombe O. & Verges J. (2012) - *Building the Zagros collisional orogen: timing, strain distribution and the dynamics of Arabia/Eurasia plate convergence*. Tectonophysics, **532**: 27-60.

Oberlander T. M. (1965) - *The Zagros streams: a new interpretation of transverse drainage in an orogenic zone*. Syracuse Geographical Series.

Oberlander T. M. (1985) - *Origin of drainage transverse to structures in orogens.* In Tectonic geomorphology, **15**: 155-182. Allen and Unwin Boston.

Parise M. & Jibson R. W. (2000) - *A seismic landslide susceptibility rating of geologic units based on analysis of characteristics of landslide triggered by the 17 January, 1994 Northridge, California earthquake*. Engineering geology, **58** (3-4): 251-270.

Paul A., Hatzfeld D., Kaviani A., Tatar M. & Pequegnat C. (2010) - *Seismic imaging of the lithospheric structure of the Zagros mountain belt (Iran).* Geological Society, London, Special Publications, **330** (1): 5-18.

Petley D. (2012) - *Global patterns of loss of life from landslides*. Geology, **40** (10): 927-930.

Pourghasemi H. R., Yansari Z. T., Panagos P. & Pradhan B. (2018) - *Analysis and evaluation of landslide susceptibility: a review on articles published during 2005–2016 (periods of 2005–2012 and 2013–2016).* Arabian Journal of Geosciences, **11** (9): 1-12.

Rajabi A. M., Mahdavifar M. R., Khamehchiyan M. & Del Gaudio V. (2011) - *A new empirical estimator of coseismic landslide displacement for Zagros Mountain region (Iran).* Natural Hazards, **59** (2): 1189-1203.

Ramsey L. A., Walker, R. T. & Jackson J. (2008) - *Fold evolution and drainage development in the Zagros mountains of Fars province, SE Iran.* Basin Research, **20** (1): 23-48.

Reichenbach P., Rossi M., Malamud B. D., Mihir M. & Guzzetti F. (2018) - *A review of statistically based landslide susceptibility models.* Earth-Science Reviews, **180**: 60-91.

Reis S., Yalcin A., Atasoy M., Nisanci R., Bayrak T., Erduran M., Sancar C. & Ekercin S. (2012) - *Remote sensing and GIS-based landslide susceptibility mapping using frequency ratio and analytical hierarchy methods in Rize province (NE Turkey).* Environmental Earth Sciences, **66** (7): 2063-2073.

Roberts N. J. & Evans S. G. (2013) - *The gigantic Seymareh (Saidmarreh) rock avalanche, Zagros Fold–Thrust Belt, Iran.* Journal of the Geological Society, **170** (4): 685-700.

Rouhi J., Delchiaro M., Della Seta M. & Martino S. (2019) - *Emplacement kinematics of the Seymareh rock-avalanche debris (Iran) inferred by field and remote surveying.* Italian Journal of Engineering Geology and Environment.

Sahabi, F. & Macleod J. H. (1969) - *Bala Rud. 1:100 000 Geological Map*. Iran Oil Operating Companies, Geological Exploration Division, Tehran, Iran.

Samia J., Temme A., Bregt A., Wallinga J., Guzzetti F. & Ardizzone F. (2020). *Dynamic path-dependent landslide susceptibility modelling.* Natural Hazards and Earth System Sciences, **20** (1): 271-285.

Sepehr M. & Cosgrove J. W. (2004) - *Structural framework of the Zagros fold–thrust belt, Iran.* Marine and Petroleum geology, **21** (7): 829-843.

Setudehnia A. (1967) - *Kuh-e Anaran. 1:100 000 Geological Map*. Iran Oil Operating Companies, Geological Exploration Division, Tehran, Iran.

Setudehnia A. & O'B Perry (1967) - *Dalpari. 1:100 000 Geological Map*. Iran Oil Operating Companies, Geological Exploration Division, Tehran, Iran.

Styron R. & Pagani M. (2020). T*he GEM global active faults database.* Earthquake Spectra, **36** (1_suppl): 160-180.

Tatar M., Hatzfeld D., Martinod J., Walpersdorf A., Ghafori-Ashtiany M. & Chery J. (2002) - *The present-day deformation of the central Zagros from GPS measurements.* Geophysical research letters, **29** (19): 33-1.

Takin M. & Macleod J. H. (1970) - *Pul and Dukthar. 1:100 000 Geological Map*. Iran Oil Operating Companies, Geological Exploration Division, Tehran, Iran.

Trigila A., Frattini P., Casagli N., Catani F., Crosta G., Esposito C., Adanza C., Lagomarsino D., Scarascia Mugnozza G., Segoni, S. Spizzichino D., Tofani V. & Lari S. (2013) - *Landslide susceptibility mapping at national scale: the Italian case study*. In Landslide science and practice: 287-295. Springer, Berlin, Heidelberg.

Trigila A., Iadanza C., Esposito C. & Scarascia Mugnozza G. (2015) - *Comparison of Logistic Regression and Random Forests techniques for shallow landslide susceptibility assessment in Giampilieri (NE Sicily, Italy)*. Geomorphology, **249**: 119-136.

U.S. Geological Survey (2020) - *Earthquake Lists, Maps, and Statistics*.

Van Westen C. J. (2000) - *The modelling of landslide hazards using GIS.* Surveys in Geophysics, **21** (2): 241-255.

Van Westen C. J., Van Asch T. W. & Soeters R. (2006) - *Landslide hazard and risk zonation—why is it still so difficult?*. Bulletin of Engineering geology and the Environment, **65** (2): 167-184.

Vakhshoori V. & Zar M. (2016) - *Landslide susceptibility mapping by comparing weight of evidence, fuzzy logic, and frequency ratio methods.* Geomatics, Natural Hazards and Risk, **7** (5): 1731-1752.

Verges J., Goodarzi M. G. H., Emami H., Karbuz R., Efstathiou J. & Gillespie P. (2011) - *Multiple detachment folding in Pusht-e Kuh arc, Zagros: Role of mechanical stratigraphy.* AAPG Bulletin.

Yamini-Fard F., Hatzfeld D., Tatar M. & Mokhtari M. (2006) - *Microearthquake seismicity at the intersection between the Kazerun fault and the Main Recent Fault (Zagros, Iran).* Geophysical Journal International, **166**: 186–196.

Whipple K. X. & Tucker G. E. (1999) - *Dynamics of the stream-power river incision model: Implications for height limits of mountain ranges, landscape response timescales, and research needs.* Journal of Geophysical Research: Solid Earth, **104** (B8): 17661-17674.

Received February 2021 - Accepted June 2021